

Optimization-Based Single Anchor UWB Positioning System for Mobile Robots

Xidong Zhou[✉], Hang Zhong[✉], Member, IEEE, Hui Zhang[✉], Yiming Jiang[✉], and Yaonan Wang[✉]

Abstract—In recent years, ultra-wideband (UWB) technology has found extensive applications in indoor positioning systems (IPS). However, a significant challenge for achieving low-cost positioning solutions is the requirement of three or more anchors in most existing UWB positioning methods. In this article, we propose a method that achieves mobile robot localization using only a single anchor. To solve for the initial positioning of the robot, we construct a factor graph composed of multiple sets of odometry position and UWB distance measurements, which is then solved through graph optimization. The robot's tracking problem can be transformed into solving a system of equations with inequality constraints. We propose an adaptive trust region algorithm for solving a system of equations jointly composed of preprocessed UWB distance measurements, odometry increments, and kinematic constraints. The trust region radius is adaptively adjusted according to the robot's motion model, leading to the iterative determination of the robot's optimal position. Experimental results demonstrate that this system achieves a high level of localization accuracy.

Index Terms—Graph optimization, mobile robot, single anchor, trust region.

I. INTRODUCTION

STATE estimation stands out as a critical module in the navigation applications of mobile robots. Achieving high-precision localization indoors, where the use of global satellite navigation systems [1] is not feasible, remains a challenging task. Currently, mainstream indoor positioning systems (IPS) [2] include wireless local area network, radio frequency identification (RFID), ultrasonic, Bluetooth, inertial, and ultra-wideband (UWB). Among these, RFID, ultrasonic, Bluetooth, and UWB are beacon-based positioning methods. Generally, RFID and Bluetooth can achieve meter-level

Received 29 May 2024; revised 14 September 2024; accepted 19 September 2024. Date of publication 16 October 2024; date of current version 1 November 2024. This work was supported in part by the National Key Research and Development Program of China under Grant 2022YFB4701800 and Grant 2021ZD0114503; in part by the National Natural Science Foundation of China under Grant U22A2057, Grant 62027810, and Grant 62103140; in part by the Major Research Plan of the National Natural Science Foundation of China under Grant 92148204; in part by Hunan Leading Talent of Technological Innovation under Grant 2022RC3063; in part by the Top Ten Technical Research Projects of Hunan Province under Grant 2024GK1010; in part by the Key Research and Development Program of Hunan Province under Grant 2023GK2068 and Grant 2022GK2011; in part by the Science and Technology Innovation Program of Hunan Province under Grant 2023RC1049; in part by the National Natural Science Foundation of JiangXi Province under Grant 2023BAB21023; and in part by the Key Research and Development Program of Jiangxi Province under Grant 2024BBG71017. The Associate Editor coordinating the review process was Dr. Gabriele Patrizi. (*Corresponding author: Hang Zhong.*)

The authors are with the School of Robotics, Hunan University, Changsha, Hunan 410082, China (e-mail: zhonghang@hnu.edu.cn).

Digital Object Identifier 10.1109/TIM.2024.3481589

positioning accuracy, while Ultrasonic and UWB can reach decimeter-level accuracy. However, higher positioning accuracy often comes at the cost of higher deployment expenses, which means more beacons or anchors are required. As UWB is one of the most widely used and highest precision IPS available today, studying single-anchor UWB positioning systems is of significant importance.

However, in traditional single-anchor UWB positioning schemes, achieving higher localization accuracy typically involves higher hardware costs (such as antenna arrays) and deployment costs (e.g., environmental mapping). Therefore, the goal of this study is to achieve higher localization accuracy with a more cost-effective solution. To this end, we adopted a two-stage approach, dividing the single-anchor UWB positioning system into two phases to enable real-time tag localization. The first phase involves the derivation of the initial coordinates of the tag, while the second phase utilizes the solution from the first phase as the initial value for the tracking algorithm, facilitating continuous tracking of the tag.

The primary objective of this study is to achieve position estimation for a mobile robot in a single-anchor UWB positioning system through optimization methods. In our previous work, we investigated methodological approaches such as Kalman filtering (KF) [3] and particle filtering (PF) [4] in multianchor UWB positioning systems, as well as an improved PF localization method in a single-anchor UWB positioning system [5]. In contrast, the optimization method proposed in this article allows for a higher precision in position estimation. Fig. 1 illustrates the single-anchor UWB positioning system based on optimization methods.

In the first phase, we construct a factor graph consisting of multiple sets of odometry position and UWB distance measurements. The initial position of the robot are then determined through graph optimization. In the second phase, we formulate a system of equations by combining preprocessed UWB distance measurements, odometry increments, and kinematic constraints. Subsequently, an adaptive trust region algorithm proposed in this article is employed to obtain the optimal solution for this system with inequality constraints. Thus, we transform the problems of initial position solution and continuous tracking in the single-anchor positioning system into solving optimization problems.

In summary, the contributions of this article are listed as follows:

- 1) In the initial position solution phase, we constructed a factor graph using odometer position and UWB dis-

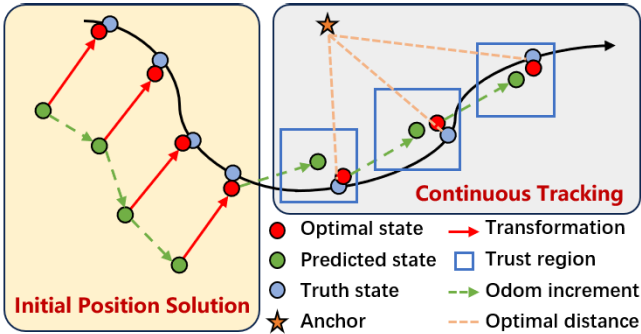


Fig. 1. Framework of a single-anchor UWB positioning system based on an optimization method.

tance measurements. By employing graph optimization techniques, we determined the optimal solution, thereby obtaining a higher precision initial position for the mobile robot. This advancement further enhances the accuracy of the single-anchor UWB positioning system.

- 2) Due to the multipath effect, UWB distance measurements are prone to errors, which can further impact positioning accuracy. Therefore, during the tracking phase, KF is applied to preprocess UWB distance measurements, mitigating the errors caused by the multipath effect. This preprocessing improves the accuracy of the observations, thereby enhancing the precision of the optimization method and reducing the error in position estimation.
- 3) We introduced an adaptive trust region algorithm. This algorithm leverages kinematic constraints to confine the solution space of the optimization method. Additionally, the trust region's radius is adaptively adjusted based on the motion model of the mobile robot, achieving high-precision localization for the mobile robot.

The remaining structure of this article is organized as follows. Section II provides a summary of relevant work on single-anchor UWB positioning systems. Section III introduces the trust region algorithm. Section IV outlines the proposed methodology. Experimental validation and discussions are presented in Section V, while Section VI concludes this article.

II. RELATED WORKS

The single-anchor UWB positioning system primarily employs three methods: an antenna array, multipath component (MPC) measurement, and two-stage positioning method. The use of antenna arrays allows for the joint estimation of the angle of arrival and time of arrival of the signal. This method conducts both range estimation and angle estimation at the anchor to locate the tag, which is typically used in multiagent cooperative positioning systems [6], visual inertial odometry [7], and 3-D target localization [8], [9]. In contrast, the latest research on the MPC method [10], [11] does not require any time-consuming setup phase, as it does not necessitate prior calibration, training, or position estimations (neither fingerprint-based [12] nor learning algorithm-based [13]). During the measurement phase, no additional external information is needed, such as prior position estimates or multiple

antennas. The only required external information is a floor plan of the localization environment, which should depict the geometry of the building where the system is installed. However, in scenarios where a floor plan cannot be provided (e.g., outdoor or open indoor environments), the MPC method becomes ineffective. Therefore, this article focuses exclusively on the two-stage positioning method. The specific related work is as follows.

A. Initial Position Solution

In single-anchor UWB positioning systems, initial position solution relies on trilateration, a distance-based positioning technique. Trilateration is based on the principle of calculating a unique point using measurements from three circles [14]. The basic concept involves selecting at least three known points in space and measuring the distances from the target object to these points. Using this distance information, a set of spheres with known points as centers and distances as radii is constructed. The target object is located at the intersection of these spheres, as its distance to each known point equals the radius of the corresponding sphere. For instance, in [15] and [5], equations are formulated using three sets of UWB distance measurements, and the coordinates of the anchor are determined using the least squares method.

To further enhance the accuracy and reliability of the solution, employing more known points (four or more) and utilizing optimization methods can be advantageous. For example, Guo et al. [16], [17] investigated a relative localization algorithm for drones. In the initial phase, a drone is required to maintain static hovering as a beacon (akin to a fixed anchor), allowing for the determination of the initial coordinates of other drones relative to the beacon. They employed multiple sets of UWB distance measurements to construct an error function and utilized the Gauss–Newton method [18] for solving. Nguyen et al. [19] proposed a tightly coupled fusion method involving a monocular camera, IMU, and a single unknown UWB anchor. The Levenberg–Marquardt method [20], [21] was employed to solve for the coordinates of the unknown anchor. Penggang et al. [22], aiming for single-anchor positioning in multiroom and multicorridor scenarios, also utilized optimization methods for anchor position determination. They initially solved for the anchor's initial values through three sets of UWB distance measurements and subsequently optimized the anchor's coordinates with a substantial number of additional UWB distance measurements to achieve more precise results.

B. Tracking

In the tracking phase of a single-anchor UWB positioning system, the current mainstream solution involves employing filtering algorithms for robust tag localization. In solutions based on the KF, Batista et al. [23] successfully estimated the system's state using the classical KF. Cao et al. [24] proposed a method that combines nine-DOF IMU and UWB for velocity estimation, employing the Extended Kalman Filtering (EKF) algorithm for tracking tasks. Penggang et al. [22] went a step further by incorporating six-DOF IMU for target localization.

Similarly, in the relative localization algorithm studied by Guo et al. [16], [17], the EKF was utilized for the state estimation of drones.

The utilization of PF for pedestrian localization in a single-anchor UWB positioning system was first introduced by Tian et al. [25]. They initially proposed a fusion method of IMU and UWB based on PF [25]. This approach solely relies on UWB distance measurements between mobile node and anchor to achieve Pedestrian Dead Reckoning (PDR). Building on this research, they later proposed a method to infer the unknown positions of UWB anchor through PDR position estimation and triangulation [15]. Furthermore, addressing the drawbacks of PF in PDR, they introduced a new particle reset method [26], resolving issues related to track lost during localization. Additionally, to mitigate errors caused by nonline-of-sight (NLOS) in UWB, they proposed an adaptive UWB ranging uncertainty model [27], enhancing the overall positioning accuracy.

III. PROPOSED METHOD

A. Overview

In this study, we employ an optimization method to estimate the robot's position. We define the anchor's position as the origin of the global coordinate system. The power-on position of the mobile robot is designated as the origin of the robot coordinate system, and the robot coordinate system is aligned with the global coordinate system through rotation transformation [5]. The specific implementation of a single-anchor UWB positioning system is illustrated in Fig. 2. It is primarily divided into three modules: initialization, preprocessing, and solving. During the initial position solution phase, the initialization module is utilized to acquire the robot's initial global coordinates. Throughout the tracking phase, the preprocessing and solving modules collaborate to determine the real-time optimal position of the robot.

In the initialization module, we use the Levenberg–Marquardt method [20], [21] to solve the factor graph constructed from odometry position and UWB distance measurements. Through coordinate transformations, we obtain the initial global coordinates of the robot. In the preprocessing module, the original UWB distance measurements are preprocessed using KF [28] based on the robot's motion model, resulting in highly accurate distance values. In the solving module, we utilize the proposed adaptive trust region algorithm to solve the optimal position of the robot, ensuring robust and high-precision continuous tracking.

In Sections III-B–III-D, the details of the initialization module, preprocessing module, and solving module are described.

B. Initialization

In the single-anchor UWB positioning system, achieving continuous tracking requires solving for the initial global coordinates of the robot. The accuracy of the initial global coordinates can significantly impact the error of the positioning system. The process of solving for the initial global

coordinates can be described as a least-squares optimization problem.

The traditional method for solving initial global coordinates is through triangulation. This method entails formulating a system of equations by amalgamating odometry position from three distinct lines with their corresponding UWB distance measurements. Although the least-squares method can be used to estimate the optimal position with the least error, relying solely on three observations cannot guarantee the accuracy of the robot's initial global coordinates. Therefore, this method still has significant limitations and inaccuracies.

Building upon the triangulation method, this study constructs an error function using all the odometry position and UWB measurements among the three sets of coordinates, and subsequently solves this error function. Thus, the original problem of solving three sets of equations is transformed into an optimization problem of multiple sets of error functions. This approach significantly enhances the accuracy of coordinate estimation. The least-squares optimization problem can be described as follows:

$$\hat{X} = \arg \min_X \sum_{i=1}^n \|e(X_i, Z_i)\|^2 \quad (1)$$

where $e(\cdot)$ represents the error between the state variable X_i and the observation variable Z_i . \hat{X} represents the optimal state that minimizes the sum of squared errors of the error functions.

The problem of solving the initial global coordinates of a robot is fundamentally a problem of coordinate transformation between the robot coordinate system and the global coordinate system. Then, the initial global coordinates are solved through the coordinate transformation matrix

$$\begin{bmatrix} \hat{x}_i \\ \hat{y}_i \\ 1 \end{bmatrix} = \begin{bmatrix} \cos \theta & -\sin \theta & u \\ \sin \theta & \cos \theta & v \\ 0 & 0 & 1 \end{bmatrix} \cdot \begin{bmatrix} x_i \\ y_i \\ 1 \end{bmatrix} \quad (2)$$

where (u, v) represents the coordinates of the origin of the robot coordinate system in the global coordinate system (the transformation to be solved), θ represents the rotation angle of the robot coordinate system relative to the global coordinate system (which is 0 in this article), (x_i, y_i) represents the coordinates in the robot coordinate system, and (\hat{x}_i, \hat{y}_i) represents the optimal position in the global coordinate system.

The solution process is shown in Fig. 3. First, assume that the robot coordinate system coincides with the global coordinate system. And set the robot's initial global coordinates as the odometer position. The error function is

$$e(X_i, Z_i) = \sqrt{x_i^2 + y_i^2} - Z_i. \quad (3)$$

Because each UWB distance measurement can get an error. Therefore, an optimal transformation matrix $[u, v]$ between coordinate systems can be found to minimize the error.

In this article, the method based on graph optimization is used to solve the initial global coordinates of the robot. Take $[u, v]$ in the transformation matrix as the vertex (optimization variable), the UWB distance measurements as the unary edge (observation equation), and $e(X_i, Y_i)$ as the error of the edge. Finally, the Levenberg–Marquardt method is used to solve the problem.

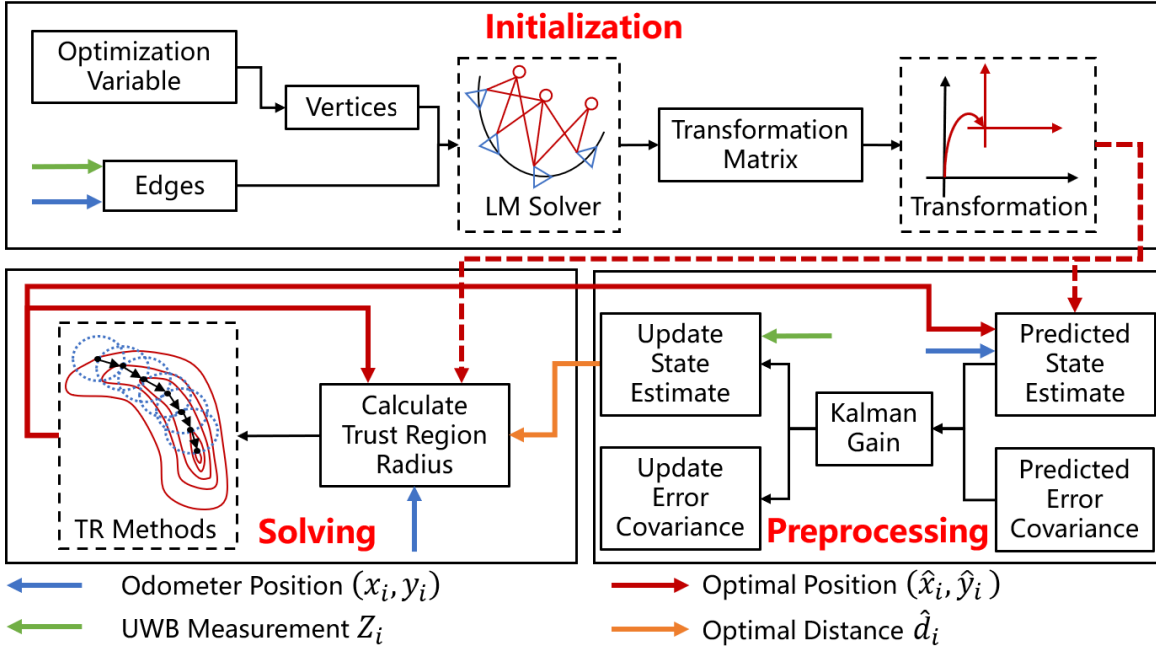


Fig. 2. Illustration of a positioning system based on optimization methods. We divide the initial position solution phase and tracking phase into initialization module, preprocessing module, and solving module.

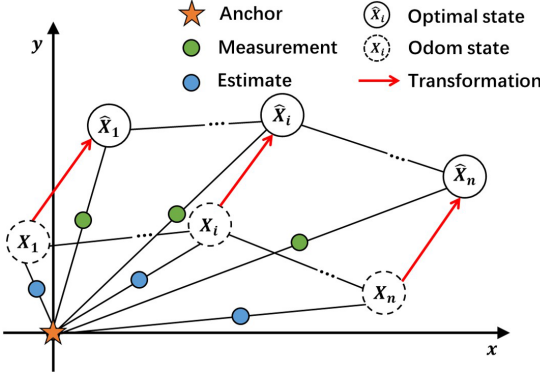


Fig. 3. Process of constructing factor graphs. The blue circle represents the estimated distance between the robot and the anchor as calculated by the odometry. The green circle represents the real distance between the robot and the anchor measured by UWB.

C. Preprocessing UWB Measurements With Kalman Filter

The error in UWB distance measurements has a significant impact on the accuracy of a single-anchor UWB positioning system. Therefore, it is necessary to apply filtering techniques to the UWB distance measurements. In this study, the robot's odometry motion model is employed to estimate the robot's current position. The distance between this estimated position and the anchor is the predicted value. By filtering the predicted values with the UWB distance measurements, the optimal distance between the anchor and the robot is obtained.

The prior estimated distance d'_i is given by

$$d'_i = \sqrt{(\hat{x}_{i-1} + \Delta x)^2 + (\hat{y}_{i-1} + \Delta y)^2}. \quad (4)$$

The prior estimation covariance is given as

$$P'_i = AP_{i-1}A^T + Q \quad (5)$$

where Q is the covariance of the process noise. Due to the changes in UWB measurements between consecutive frames being minimal, simplifying it to a static model, the state transition matrix $A = 1$.

The Kalman Gain is given by

$$K = \frac{P'_i H^T}{(H P'_i H^T + R)} \quad (6)$$

where R is the covariance of measurement noise. Since the observed value (UWB measurement) directly corresponds to the state value (distance), the observation matrix $H = 1$.

The optimal estimation is given by

$$\hat{d}_i = d'_i + K(Z_i - Hd'_i). \quad (7)$$

The covariance of the posterior estimation is

$$P_i = (1 - KH)P'_i. \quad (8)$$

During the initial entry into the tracking phase, the KF inputs the optimal coordinates $(\hat{x}_{i-1}, \hat{y}_{i-1})$ from the previous time step, which are derived during the initial position solution phase. In subsequent entries into the tracking phase, $(\hat{x}_{i-1}, \hat{y}_{i-1})$ are the solutions obtained by Section III-D adaptive trust region algorithm.

D. Solving With Adaptive Trust Region Method

Assuming the current coordinates of a robot are given by $X = (x, y)$. In an ideal scenario with no errors, the distance between the assumed coordinates X and an anchor should be equal to the optimal distance value \hat{d}_i . The difference between the assumed coordinates X and the optimal coordinates from the previous time step $(\hat{x}_{i-1}, \hat{y}_{i-1})$ should satisfy the odometry increments Δx and Δy . Based on this, we can formulate a system of quadratic equations.

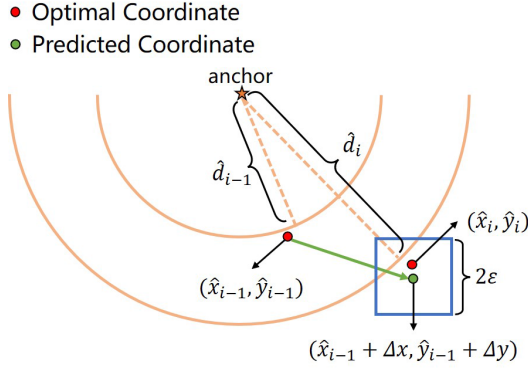


Fig. 4. Solution process with inequality constraints. The green circle represents the predicted coordinates obtained by the odometry increment (the initial value of the solution). The blue rectangle represents the trust region radius (solution range). The yellow curve represents the optimal distance value.

The observation equation can be expressed as

$$X(1)^2 + X(2)^2 = \hat{d}_i^2. \quad (9)$$

The prediction equation can be expressed as

$$\begin{cases} (X(1) - \hat{x}_{i-1})^2 + (X(2) - \hat{y}_{i-1})^2 = \Delta x^2 + \Delta y^2 \\ X(2) - \hat{y}_{i-1} = \frac{\Delta y}{\Delta x} \cdot (X(1) - \hat{x}_{i-1}). \end{cases} \quad (10)$$

The above system of equations constitutes a nonlinear optimization problem. The incremental data from the odometry is highly accurate over short periods, allowing the predicted coordinates to be used as initial values for equation solving. However, due to the significant impact of observation errors on the accuracy of the solution, it is necessary to introduce a constraint ε to the system of equations

$$\begin{cases} \hat{x}_{i-1} + \Delta x - \varepsilon \leq X(1) \leq \hat{x}_{i-1} + \Delta x + \varepsilon \\ \hat{y}_{i-1} + \Delta y - \varepsilon \leq X(2) \leq \hat{y}_{i-1} + \Delta y + \varepsilon. \end{cases} \quad (11)$$

By introducing ε , the solution process is constrained to occur only in the vicinity of the highly accurate predicted position, as depicted by the blue box in Fig. 4. This transformation effectively converts the localization problem into solving equations with inequality constraints.

The trust region algorithm derives iterations by iteratively solving the corresponding optimization problem within a bounded region [29]. The trust region approach is strongly associated with approximation. Assuming we have a current guess x_k for the solution to the optimization problem $\min f(x)$, we can construct an approximate model $f(x_k + s)$ around the current point. The solution of this approximate model can then serve as the next iteration point. However, in the trust region algorithm, the approximate model is only “trusted” in a certain region around the current iteration. The region that the approximate model is trusted is called the trust region Ω_k , and the range of this region is called the trust region radius Δ_k . Ω_k is adjusted at each iteration. Therefore, the trust region algorithm can effectively solve problems with inequality constraints.

The trust region can be represented as

$$\Omega_k = \{x \in R^n | \|x - x_k\| \leq \Delta_k\}. \quad (12)$$

Algorithm 1 Adaptive Trust Region Algorithm

Require:

$$\begin{aligned} f(\cdot) &\leftarrow \text{according (9) (10)} \\ X &= (\hat{x}_{i-1} + \Delta x, \hat{y}_{i-1} + \Delta y) \\ \eta_1, \eta_2, \epsilon & \end{aligned}$$

Ensure:

```

1: // Calculate trust region radius
2: ε ← according (19)
3: Δ ← ε
4: while 1 do
5:   // Calculate Jacobian matrix and Hessian matrix
6:   g ← ∇f(X), H ← ∇²f(X)
7:   // Determine whether convergence
8:   if ‖g‖ < ε then
9:     break
10:  end if
11:  // Solving the optimal solution of the subproblem
12:  min φ_k(s) ← according (14)
13:  // Calculate trust region fidelity
14:  r ← according (15)
15:  // Update X and Δ
16:  if r ≤ η₁ then
17:    Δ ← τ₁Δ
18:  else
19:    X ← X + s
20:    if r ≤ η₂ then
21:      Δ ← τ₁Δ
22:    else
23:      Δ ← τ₂Δ
24:    end if
25:  end if
26: end while
27: // Output optimal coordinates
28: (x̂_i, ŷ_i) ← X

```

The approximate model can be represented as

$$f(x_k + s) = f(x_k) + g_k^T s + \frac{1}{2} s^T H_k s \quad (13)$$

where $g_k = \nabla f(x_k)$ is the Jacobian matrix of f at x_k , and $H_k = \nabla^2 f(x_k)$ is Hessian matrix of f at x_k .

The subproblem of trust region algorithm is defined as

$$\begin{cases} \min_{s \in R^n} \phi_k(s) = g_k^T s + \frac{1}{2} s^T H_k s \\ \text{s.t. } \|s\|_2 \leq \Delta_k. \end{cases} \quad (14)$$

After solving the solution of the subproblem, it is necessary to evaluate whether the optimal solution s_k is acceptable. Trust region fidelity is defined as

$$r_k = \frac{\text{Pred}_k}{\text{Ared}_k} \quad (15)$$

where $\text{Pred}_k = \phi_k(0) - \phi_k(s_k)$ is the predicted reduction, and $\text{Ared}_k = f(x_k) - f(x_k + s_k)$ is the actual reduction. r_k is used to measure the consistency between the approximate model and the objective function, so as to decide whether to adjust the new trust region radius.

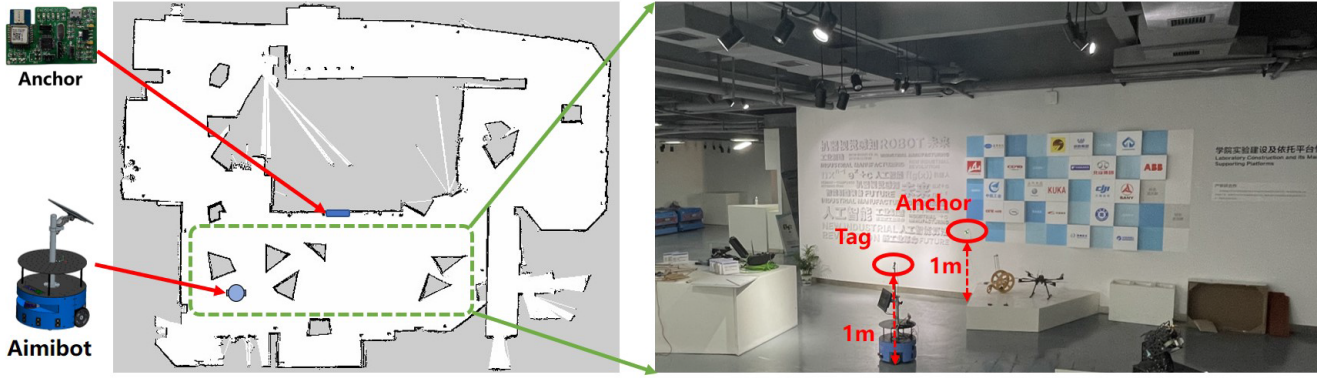


Fig. 5. Experimental site and map. The green rectangle is the Aimibot's motion area.

The x_{k+1} and Δ_{k+1} can be updated as follows:

$$x_{k+1} = \begin{cases} x_k, & r_k \leq \eta_1 \\ x_k + s_k, & r_k > \eta_1 \end{cases} \quad (16)$$

$$\Delta_{k+1} = \begin{cases} \tau_1 \Delta_k, & r_k \leq \eta_2 \\ \tau_2 \Delta_k, & r_k > \eta_2 \end{cases} \quad (17)$$

The typical values for the constants η_1 , η_2 , and τ_i are $\eta_1 = 0$, $\eta_2 = 0.25$, $\tau_1 = 0.5$, and $\tau_2 = 2$ [30]. Repeat the above steps until the sequence of iterates $\{x_k\}$ converges.

To enhance the robustness of the positioning system, this article proposes an adaptive trust region algorithm. This algorithm dynamically adjusts the trust region radius by evaluating the errors between predicted values and observed values. The evaluation metric can be expressed as follows:

$$\delta = \sqrt{(\hat{x}_{i-1} + \Delta x)^2 + (\hat{y}_{i-1} + \Delta y)^2} - \hat{d}_i. \quad (18)$$

The trust region radius is selected based on the evaluation metric δ

$$\varepsilon = \begin{cases} \alpha, & a < \delta \\ \alpha \cdot \delta, & \beta/\alpha \leq \delta \leq \alpha \\ \beta, & \delta < \beta/\alpha \end{cases} \quad (19)$$

where $0 < \beta < \alpha$. Therefore, the value range of the trust region radius is fixed between $[\beta, \alpha]$.

The adaptive trust region algorithm pseudo code is shown in Algorithm 1.

IV. EXPERIMENTS

A. Devices and Experimental Setup

The Aimibot mobile robot platform was utilized for this experiment. Aimibot employs a two-wheeled differential drive system and is equipped with reversible dc motors, high-resolution motion encoders, and batteries. Additionally, it is outfitted with an ultrasonic sensor, an anti-drop sensor, an IMU, and a Jetson Nano onboard computer.

In this experiment, we use the DW1000 UWB chip and STM32F1 minimum system as a node. The STM32 communicates with the DW1000 via the SPI protocol and controls the DW100 for data transmission and reception. After obtaining the corresponding timestamps, we calculate the difference in

Time of flight (TOF) and get the average TOF. Multiply it by the flight speed. We then get the distance. As the DW1000 has some systematic errors, the DW1000 needs to be externally calibrated using the method in [4] for both DW1000 chips. Finally, the distance data are brought into the calibration formula to obtain the exact distance between the two nodes. The mobile node communicates with the Aimibot through RS232. The processing platform of the Aimibot reads the distance data obtained from the tag. We utilized the robot operating system (ROS) to publish topics for UWB measurement distances and odometry position. A terminal server within the same local network is subscribed to topics published by Aimibot, recording all data using MATLAB.

The experiment is divided into two parts: the initial position solution experiment and the tracking experiment. The experiment took place in the exhibition hall of Building C1 at the School of Robotics, Hunan University. Anchor and tag were positioned at the same height, 1 m above the ground. This elevation surpasses all obstacles within the Aimibot's operational area, effectively eliminating the impact of NLOS communication issues between anchor and tag. We employed the open-source mapping algorithm Gmapping [31] in ROS to map the entire experimental area. To ensure experimental convenience, we overlaid the map coordinate system with the global coordinate system. The experimental site and map are illustrated in the Fig. 5.

B. Results and Discussions

To validate the effectiveness of the initial position solution, we had the Aimibot move randomly from different initial positions within the motion area of the experimental site. When the motion trajectory of Aimibot satisfies the conditions for solving triangulation with three sampled points [15], we combine all the UWB distance measurements and odometry position between these three sampled points using (7) and (9). Subsequently, we employ the Levenberg–Marquardt method from the open-source graph optimization framework g2o [32] for solving. Finally, coordinate transformation is performed using (8).

We conducted a comparative analysis between the graph optimization method and triangulation method, and the trajectories are depicted in Fig. 6. It is evident that as the number of

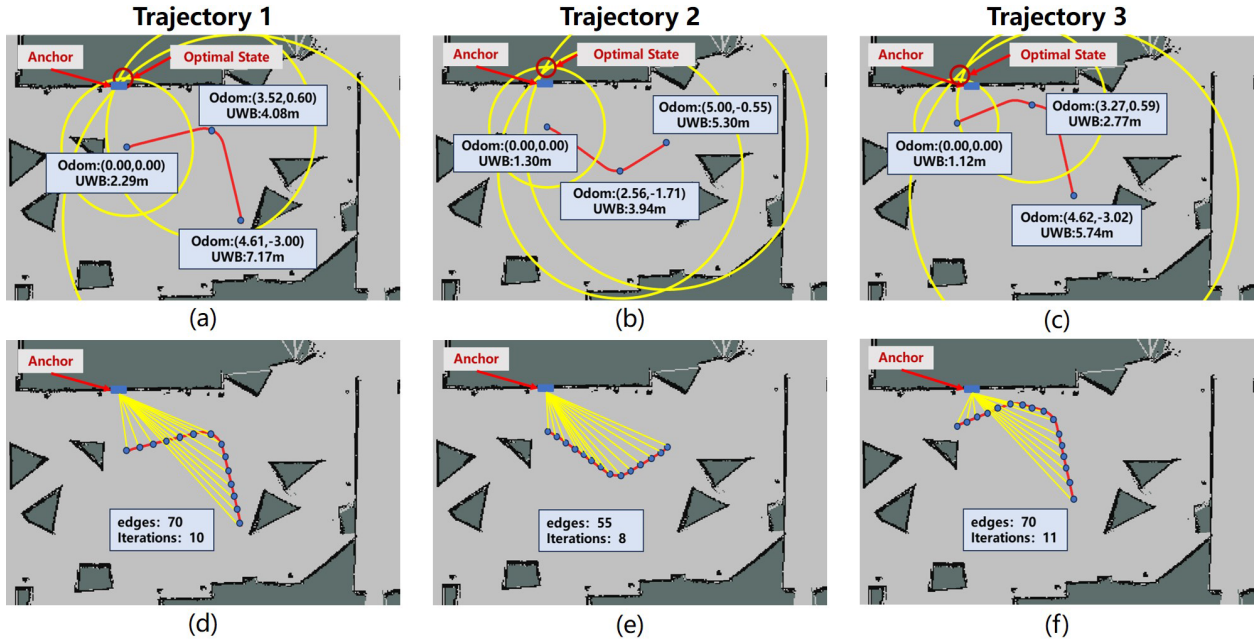


Fig. 6. Trajectories and solutions comparison between the optimization method and the triangulation method during the initial position solution phase. (a)–(c) Correspond to the solutions obtained using the triangulation method. (d)–(f) Depict the solutions achieved through the optimization method.

TABLE I
ERROR FOR INITIAL POSITION SOLUTION

	Trajectory 1	Trajectory 2	Trajectory 3
Initial Position (m)	(0.20, -2.30)	(0.00, -1.30)	(-0.50, -1.00)
Triangulation (m)	(0.19, -2.34)	(0.00, -1.38)	(-0.54, -1.04)
Error (m)	0.041	0.080	0.056
Optimization (m)	(0.18, -2.31)	(0.01, -1.31)	(-0.53, -1.01)
Error (m)	0.022	0.014	0.031
Number of Points	71	56	71

TABLE II
PARAMETER SETTINGS

Parameter	Value
α	0.01
β	0.1
η_1	0.05
η_2	0.9
τ_1	0.5
τ_2	2

edges in the graph optimization method increases, the iteration count also rises. However, convergence conditions can be achieved with approximately ten iterations. The error results are presented in Table I. Under the same motion trajectory, the initial position solution accuracy based on the graph optimization method is superior. The average error for the triangulation method is 0.059 m, while the graph optimization method yields an average error of 0.022 m. Experimental results indicate that the optimization method achieves higher localization accuracy by utilizing additional previously unused measurement data, without requiring an increase in the trajectory length compared to the triangulation method.

Subsequently, we conducted the tracking experiment. As this experimental segment primarily focuses on comparing the accuracy of tracking algorithms, it is crucial to ensure that the initial values for different tracking algorithms are consistent. We set the initial position for the tracking experiment at $(-5, -5)$.

The parameter settings for the adaptive trust region algorithm are shown in the Table II. Here, α represents the maximum radius of the trust region to prevent it from

becoming excessively large (indicating the maximum error typically encountered by the positioning system). β denotes the minimum radius of the trust region to prevent it from becoming too small (indicating the minimum error typically encountered by the positioning system). The parameters $\eta_1, \eta_2, \tau_1, \tau_2$ were set to typical values [30].

To obtain the actual trajectory of the Aimibot, we installed a high-precision laser radar on the Aimibot. We used the open-source localization algorithm adaptive Monte Carlo localization (AMCL) [33] in ROS to track the Aimibot in real time. The initial position of the Aimibot was obtained using a laser rangefinder to ensure the accuracy of AMCL. AMCL is currently one of the most mature and accurate indoor localization algorithms for mobile robots. Therefore, in this study, we used the output of AMCL as the ground truth trajectory of the Aimibot.

Multiple tracking experiments with varying trajectories were conducted, as illustrated in the Fig. 7. It can be observed that the adaptive trust region algorithm effectively tracks the robot. At the same time, the cumulative error of the odometry is effectively eliminated. The root mean square errors (RMSE)

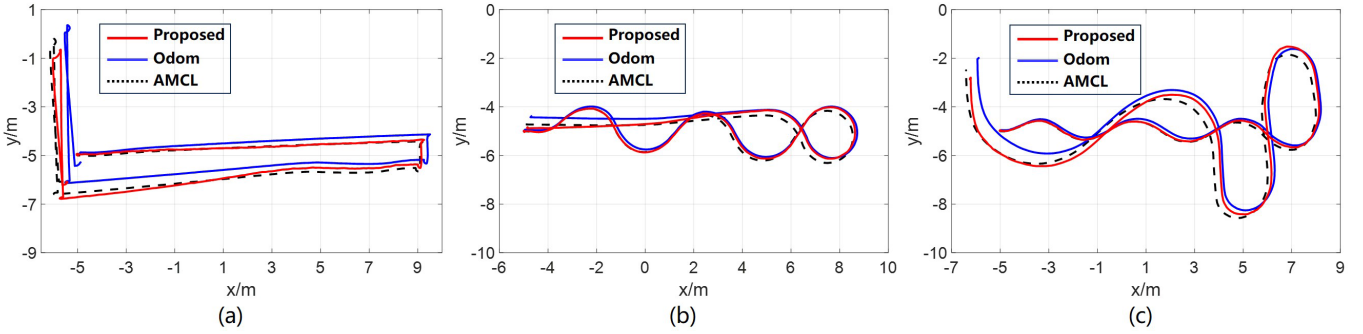


Fig. 7. (a)–(c) Comparison of the proposed method, odometer, and AMCL tracking results under different trajectories.

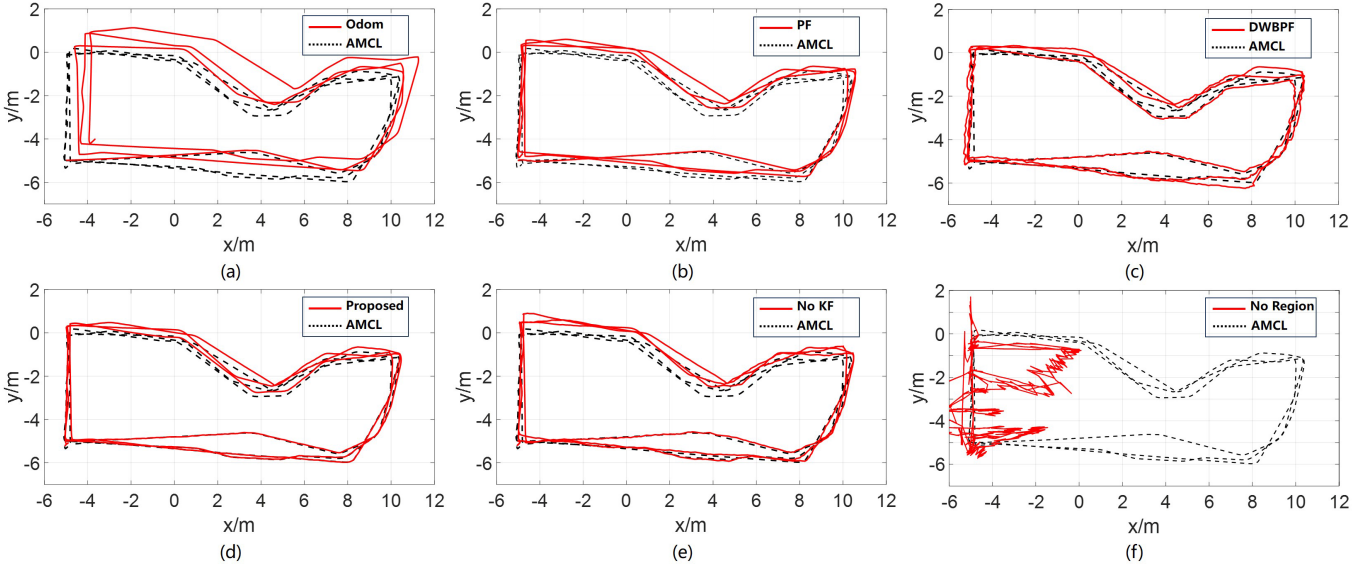


Fig. 8. Positioning trajectories of comparison experiment and ablation experiment. (a) Odometer. (b) PF. (c) DWBPF. (d) Propose method. (e) Propose method without KF. (f) Propose method without trust region.

for odometry and the optimization method for the three trajectories are 0.501/0.199, 0.241/0.162, and 0.372/0.215 m, respectively.

Next, comparative and ablation experiments were conducted. We controlled the Aimibot to traverse a predefined closed path within the motion area for three complete cycles, ultimately returning to the starting point of the motion. In single anchor UWB positioning systems, the nonlinear characteristics of UWB measurement uncertainties make PF more suitable than KF or EKF [27]. Therefore, our comparative experiments focus primarily on comparing PF with the proposed algorithm. We compared the traditional PF and our previously proposed dynamic window-based PF (DWBPF) [5]. Additionally, ablation experiments were conducted on our proposed adaptive trust region algorithm by removing the KF component (no KF) and the trust region component (no region). The positioning trajectories are illustrated in the Fig. 8.

1) Analysis of Positioning Accuracy: The absolute positioning errors of the three tracking algorithms are depicted in the Fig. 9. The RMSE for the odometry is 0.841 m, for the PF method is 0.345 m, for the DWBPF method is 0.268 m, and for the optimization method is 0.219 m. It can be observed that

compared to PF, both DWBPF and the optimization method exhibit higher accuracy. However, DWBPF's trajectory shows some jitter. On the other hand, our proposed method maintains trajectory smoothness while ensuring positioning accuracy comparable to DWBPF. This phenomenon arises because the localization output in DWBPF is the average coordinates of the highest-scoring particle set. Since the state transition of particles is a stochastic process, the particle set can only describe a certain range around the optimal coordinates of the mobile robot. The center point of this range corresponds to the optimal coordinates in DWBPF. In contrast, the optimization method directly computes the coordinates that minimize the error function, resulting in smoother trajectories compared to DWBPF.

2) Analysis of KF Component: In the absence of the KF component, the positioning trajectory of the optimization method exhibited some errors. This is attributed to the KF component's ability to mitigate UWB distance measurement errors, thereby enhancing the accuracy of observations input into the trust region algorithm. Accurate observations contribute to improved positioning accuracy. The UWB distance measurement errors before and after KF filtering are depicted in the Fig. 10.

TABLE III
SINGLE-ANCHOR POSITIONING SCHEMES COMPARISON

Schemes	Algorithms	Requirements	Sensors	Original Accuracy(m)	UWB Accuracy(m)
Antenna Array	[7]	2-Antenna Anchors Known Position of Anchors	Camera + IMU + UWB	0.18	0.05
	[9]	8-Antenna Anchors Known Position of Anchors	IMU + UWB	0.45	0.29
	[12]	Statistical Features of Multipath Components Known Position of Anchors Floor Plan	UWB	/	0.06
MPC	[10]	Known Position of Anchors Several Directional Antennas	UWB	/	0.20
	[26]	Known Robot Orientation	IMU + UWB	4.07	0.58
	DWBPF	Known Robot Orientation	Odom + UWB	0.13	0.06
Two Stage	Ours	Known Robot Orientation	Odom + UWB	0.84	0.21

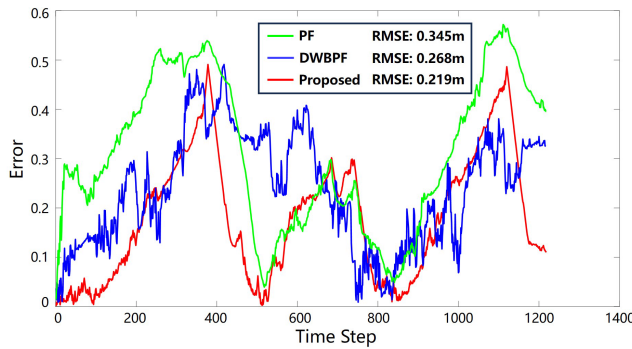


Fig. 9. RMSE for PF, DWBPF, and the proposed method.

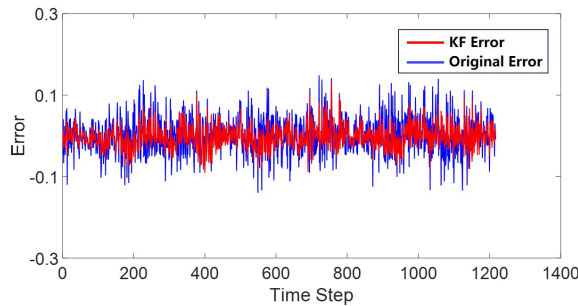


Fig. 10. UWB distance measurement errors before and after KF filtering.

3) Analysis of Trust Region Component: Without the trust region component, the positioning trajectory displayed substantial errors. This is because, without the trust region, the algorithm reduces to a general least squares optimization method, iteratively searching for the solution that minimizes error in the objective function. However, in a single-anchor positioning system, the solution with the minimum error is not necessarily the optimal position. An incorrect estimation of the current position leads to erroneous initial values for subsequent inputs into the algorithm. Since only odometry increments are used in the prediction equations, incorrect initial values result in inaccurate predictions, amplifying errors in subsequent outputs. Consequently, this leads to uncorrectable errors in the positioning trajectory. Hence, employing a trust region algorithm with boundary constraints is essential.

4) Analysis of Time Cost: The average time for one iteration of the adaptive trust region algorithm is approximately 0.01 s. In contrast, the PF method takes about 0.005 s for one iteration, exhibiting a speed nearly twice as fast as the adaptive trust region algorithm. However, given the UWB ranging frequency of around 3.57 Hz [5], it takes approximately 0.28 s to obtain one UWB distance measurement. This time interval is significantly larger than the solving time of the adaptive trust region algorithm. Therefore, despite the greater computational complexity and time cost of the adaptive trust region algorithm compared to PF, the former can still meet the real-time localization requirements in a single-anchor UWB positioning system.

Finally, our method was compared with existing single-anchor positioning schemes, including the antenna array, MPC measurement, and the two-stage positioning method, as shown in the Table III. The first two schemes require specific conditions, making them difficult to reproduce with our current hardware (single antenna) and scenario (unobstructed open indoor environment). Consequently, we focused on the improvement in positioning accuracy as a key comparison metric.

The MPC method, relying solely on UWB sensors, does not have the original sensor's positioning accuracy. Nevertheless, it attains high accuracy by processing environmental information (e.g., constructing fingerprints or obtaining floor plans), which introduces certain limitations. Moreover, both the antenna array and MPC methods necessitate the initial position of the anchor, a drawback when compared to the two-stage method. It is clear that our method significantly enhances positioning accuracy. Although there is still a gap in accuracy compared with the method in [26], this method involves offline processing and takes 2.77 s, which far exceeds our solution time. Thus, our method demonstrates superior performance within the two-stage positioning method.

V. CONCLUSION

In this article, we present an optimization method for a single-anchor UWB localization system. This system achieves high-precision tracking of a mobile robot solely based on UWB distance measurements and the robot's odometry. In the

initial position solving approach of this article, a factor graph is constructed using odometry position and UWB distance measurements. Subsequently, the accurate initial position of the mobile robot is determined through graph optimization techniques. During the tracking phase, we initially preprocess UWB distance measurements using KF. Subsequently, the proposed adaptive trust region algorithm robustly tracks the movement of the mobile robot. Experimental results demonstrate the excellent positioning performance of the optimization method in both the initial position solving and tracking phases.

The methodology proposed in this article does not consider applications in NLOS scenarios. Therefore, our future work will focus on incorporating additional anchor points or integrating NLOS detection and mitigation methods into the optimization process to address the impact of NLOS on positioning accuracy.

REFERENCES

- [1] A. Waadt, G. H. Bruck, and P. Jung, "An overview of positioning systems and technologies," in *Proc. 2nd Int. Symp. Appl. Sci. Biomed. Commun. Technol.*, Nov. 2009, pp. 1–5.
- [2] L. Batistic and M. Tomic, "Overview of indoor positioning system technologies," in *Proc. 41st Int. Conv. Inf. Commun. Technol., Electron. Microelectron. (MIPRO)*, May 2018, pp. 473–478.
- [3] T. Xu et al., "A weight adaptive Kalman filter localization method based on UWB and odometry," in *Proc. Int. Conf. Adv. Robot. Mechatronics (ICARM)*, 2022, pp. 956–961.
- [4] X. Zhou, H. Zhang, X. Tan, and J. Zhang, "A location method based on UWB for ward scene application," in *Proc. 36th Youth Acad. Annu. Conf. Chin. Assoc. Automat. (YAC)*, 2021, pp. 66–71.
- [5] H. Zhang et al., "A dynamic window-based UWB-odometer fusion approach for indoor positioning," *IEEE Sensors J.*, vol. 23, no. 3, pp. 2922–2931, Feb. 2023.
- [6] Y. Liu, R. Yan, B. Lian, and H. Zhao, "Hybrid IMU/UWB cooperative localization algorithm in single-anchor networks," *IEEE Geosci. Remote Sens. Lett.*, vol. 19, 2022, Art. no. 3511605.
- [7] Y. Zhang, J. Li, and S. Zhao, "Fusion positioning of ultra-wideband single base station and visual inertial odometry based on arrival of angle and time of flight," in *Proc. 2nd Int. Conf. Robot., Artif. Intell. Intell. Control (RAIIC)*, 2023, pp. 365–371.
- [8] B. Sun et al., "A reliable and efficient UWB-based indoor localization scheme," in *Proc. IEEE 15th Int. Conf. Adv. Infocomm Technol. (ICAIT)*, Oct. 2023, pp. 186–191.
- [9] F. Ge and Y. Shen, "Single-anchor ultra-wideband localization system using wrapped PDoA," *IEEE Trans. Mobile Comput.*, vol. 21, no. 12, pp. 4609–4623, Dec. 2022.
- [10] B. Großwindhager et al., "SALMA: UWB-based single-anchor localization system using multipath assistance," in *Proc. 16th ACM Conf. Embedded Netw. Sensor Syst.*, 2018, pp. 132–144.
- [11] S. O. Schmidt, M. Cimdins, F. John, and H. Hellbrück, "SALOS—A UWB single-anchor indoor localization system based on a statistical multipath propagation model," *Sensors*, vol. 24, no. 8, 2024. [Online]. Available: <https://www.mdpi.com/1424-8220/24/8/2428>
- [12] H. Mohammadmoradi, M. Heydariaan, O. Gnawali, and K. Kim, "UWB-based single-anchor indoor localization using reflected multipath components," in *Proc. Int. Conf. Comput., Netw. Commun. (ICNC)*, Feb. 2019, pp. 308–312.
- [13] S. Li, A. Balatsoukas-Stimming, and A. Burg, "Single-anchor UWB localization using channel impulse response distributions," in *Proc. IEEE Int. Conf. Acoust., Speech Signal Process. (ICASSP)*, Jun. 2023, pp. 1–5.
- [14] C. Smith, "Three-circle problems in modern geometry," *Nat. Math. Mag.*, vol. 14, no. 6, pp. 299–307, 1940.
- [15] Q. L. Tian, K. I.-K. Wang, and Z. Salcic, "A low-cost INS and UWB fusion pedestrian tracking system," *IEEE Sensors J.*, vol. 19, no. 10, pp. 3733–3740, May 2019.
- [16] K. Guo, Z. Qiu, W. Meng, T. M. Nguyen, and L. Xie, "Relative localization for quadcopters using ultrawideband sensors," in *Proc. InternationalMicro Air Vechicle Competition Conf. (IMAV)*, 2016, pp. 243–248.
- [17] K. Guo, Z. Qiu, W. Meng, L. Xie, and R. Teo, "Ultra-wideband based cooperative relative localization algorithm and experiments for multiple unmanned aerial vehicles in GPS denied environments," *Int. J. Micro Air Veh.*, vol. 9, no. 3, pp. 169–186, 2017.
- [18] S. Kohlbrecher, O. von Stryk, J. Meyer, and U. Klingauf, "A flexible and scalable SLAM system with full 3D motion estimation," in *Proc. IEEE Int. Symp. Saf., Secur., Rescue Robot.*, Kyoto, Japan, 2011, pp. 155–160.
- [19] T. H. Nguyen, T. Nguyen, and L. Xie, "Range-focused fusion of camera-IMU-UWB for accurate and drift-reduced localization," *IEEE Robot. Autom. Lett.*, vol. 6, no. 2, pp. 1678–1685, Apr. 2021.
- [20] K. Levenberg, "A method for the solution of certain non-linear problems in least squares," *Quart. Appl. Math.*, vol. 2, no. 2, pp. 164–168, 1944.
- [21] D. Marquardt, "An algorithm for least-squared estimation of non linear parameters," *J. Soc. Ind. Appl. Math.*, vol. 11, no. 2, pp. 431–441, 1963.
- [22] G. Penggang, L. Gao, L. Yunhui, and C. Wen, "A novel method for UWB-based localization using fewer anchors in a floor with multiple rooms and corridors," in *Proc. IEEE 12th Int. Conf. Indoor Positioning Indoor Navigat. (IPIN)*, Sep. 2022, pp. 1–6.
- [23] P. Batista, C. Silvestre, and P. Oliveira, "Single range aided navigation and source localization: Observability and filter design," *Syst. Control Lett.*, vol. 60, pp. 665–673, Aug. 2011.
- [24] Y. Cao, C. Yang, R. Li, A. Knoll, and G. Beltrame, "Accurate position tracking with a single UWB anchor," in *Proc. IEEE Int. Conf. Robot. Autom. (ICRA)*, Sep. 2020, pp. 2344–2350.
- [25] Q. Tian, K. I.-K. Wang, and Z. Salcic, "Human body shadowing effect on UWB-based ranging system for pedestrian tracking," *IEEE Trans. Instrum. Meas.*, vol. 68, no. 10, pp. 4028–4037, Oct. 2019.
- [26] Q. Tian, K. I.-K. Wang, and Z. Salcic, "A resetting approach for INS and UWB sensor fusion using particle filter for pedestrian tracking," *IEEE Trans. Instrum. Meas.*, vol. 69, no. 8, pp. 5914–5921, Aug. 2020.
- [27] Q. Tian, I. Kevin, K. Wang, and Z. Salcic, "An INS and UWB fusion approach with adaptive ranging error mitigation for pedestrian tracking," *IEEE Sensors J.*, vol. 20, no. 8, pp. 4372–4381, Apr. 2020.
- [28] R. E. Kálmán, "A new approach to linear filtering and prediction problems," *J. Basic Eng.*, vol. 82, no. 1, pp. 35–45, Mar. 1960.
- [29] T.-L. Liu and H.-T. Chen, "Real-time tracking using trust-region methods," *IEEE Trans. Pattern Anal. Mach. Intell.*, vol. 26, no. 3, pp. 397–402, Mar. 2004.
- [30] Y. X. Yuan, "A review of trust region algorithms for optimization," in *Proc. ICIAM*, Edinburgh, U.K., 1999, pp. 271–282.
- [31] G. Grisetti, C. Stachniss, and W. Burgard, "Improved techniques for grid mapping with rao-blackwellized particle filters," *IEEE Trans. Robot.*, vol. 23, no. 1, pp. 34–46, Feb. 2007.
- [32] R. Kümmerle, G. Grisetti, H. Strasdat, K. Konolige, and W. Burgard, " g^2o : A general framework for graph optimization," in *Proc. IEEE Int. Conf. Robot. Autom.*, May 2011, pp. 3607–3613.
- [33] F. Dellaert, D. Fox, W. Burgard, and S. Thrun, "Monte Carlo localization for mobile robots," in *Proc. IEEE Int. Conf. Robot. Autom.*, vol. 2, May 1999, pp. 1322–1328.



Xidong Zhou received the M.S. degree from the School of Electrical and Information Engineering, Changsha University of Science and Technology, Changsha, China, in 2023. He is currently pursuing the Ph.D. degree with the School of Robotics, Hunan University, Changsha.

His research interests include path planning of mobile robots, localization, and mapping.



Hang Zhong (Member, IEEE) received the B.S., M.S., and Ph.D. degrees in automation science from the College of Electrical and Information Engineering, Hunan University, Changsha, China, in 2013, 2016, and 2020, respectively.

His research interests include aerial robotics, multirobot systems, visual servoing, visual navigation, and nonlinear control.



Yiming Jiang received the B.S. degree in automation from Hunan University, Changsha, China, in 2011, the M.S. degree in control theory and engineering from the School of Automation, Guangdong University of Technology, Guangzhou, China, in 2015, and the Ph.D. degree from the School of Control Science and Engineering, South China University of Technology, Guangzhou, in 2019.

His research interests include robotics, intelligent control, and human–robot interaction.



Hui Zhang received the B.S., M.S., and Ph.D. degrees in pattern recognition and intelligent system from Hunan University, Changsha, China, in 2004, 2007, and 2012, respectively.

His research interests include machine vision, image processing, and robot vision.



Yaonan Wang received the Ph.D. degree in electrical engineering from Hunan University, Changsha, China, in 1994.

Since 1995, he has been a Professor with the College of Electrical and Information Engineering, Hunan University. Since 2019, he has been an Academician with the Chinese Academy of Engineering. His current research interests include robotics, intelligent control, and image processing.